

Award Number: W81XWH-04-1-0240

TITLE: High Resolution Anatomic and Elastographic Transrectal
Ultrasound for Improved Diagnosis of Prostate Cancer

PRINCIPAL INVESTIGATOR: John A. Hossack, Ph.D.

CONTRACTING ORGANIZATION: Virginia University
Charlottesville, Virginia 22904

REPORT DATE: February 2005

TYPE OF REPORT: Annual

PREPARED FOR: U.S. Army Medical Research and Materiel Command
Fort Detrick, Maryland 21702-5012

DISTRIBUTION STATEMENT: Approved for Public Release;
Distribution Unlimited

The views, opinions and/or findings contained in this report are those of the author(s) and should not be construed as an official Department of the Army position, policy or decision unless so designated by other documentation.

20050712 034

REPORT DOCUMENTATION PAGE

Form Approved
OMB No. 074-0188

Public reporting burden for this collection of information is estimated to average 1 hour per response, including the time for reviewing instructions, searching existing data sources, gathering and maintaining the data needed, and completing and reviewing this collection of information. Send comments regarding this burden estimate or any other aspect of this collection of information, including suggestions for reducing this burden to Washington Headquarters Services, Directorate for Information Operations and Reports, 1215 Jefferson Davis Highway, Suite 1204, Arlington, VA 22202-4302, and to the Office of Management and Budget, Paperwork Reduction Project (0704-0188), Washington, DC 20503

1. AGENCY USE ONLY (Leave blank)	2. REPORT DATE February 2005	3. REPORT TYPE AND DATES COVERED Annual (21 Jan 2004 - 20 Jan 2005)
--	--	---

4. TITLE AND SUBTITLE High Resolution Anatomic and Elastographic Transrectal Ultrasound for Improved Diagnosis of Prostate Cancer	5. FUNDING NUMBERS W81XWH-04-1-0240
---	---

6. AUTHOR(S)
John A. Hossack, Ph.D.

7. PERFORMING ORGANIZATION NAME(S) AND ADDRESS(ES)
Virginia University
Charlottesville, Virginia 22904

E-Mail: Jh7fj@virginia.edu

8. PERFORMING ORGANIZATION REPORT NUMBER

9. SPONSORING / MONITORING AGENCY NAME(S) AND ADDRESS(ES)
U.S. Army Medical Research and Materiel Command
Fort Detrick, Maryland 21702-5012

10. SPONSORING / MONITORING AGENCY REPORT NUMBER

11. SUPPLEMENTARY NOTES

12a. DISTRIBUTION / AVAILABILITY STATEMENT
Approved for Public Release; Distribution Unlimited

12b. DISTRIBUTION CODE

13. ABSTRACT (Maximum 200 Words)

In this work we improve upon conventional Digital Rectal Examination (DRE) and PSA blood test by using ultrasound elasticity imaging. A latex sheath over the transrectal ultrasound probe is slightly inflated with water to provide a source of moderate pressure. The elasticity image is generated by cross-correlating successive raw radio frequency image data sets for incrementally increasing pressure. Strain, and consequently elasticity, can be calculated from the displacement image. Our second objective is to use a new freehand 3D acquisition approach to obtain 3D image data sets. This approach uses a slightly modified transducer and an image motion tracking technique. Preliminary phantom based results are presented in this report. Excellent progress has been made with respect to the Statement of Work and first three of four total Specific Aims. A transducer has been specified and is on order. As promised, this transducer is designed to possess unsurpassed prostate scanning resolution by virtue of its exceptionally high frequency - up to 14 MHz. Prototype phantoms and complete ultrasound test instrumentation has been assembled. Preliminary ultrasound image speckle reduction work has been performed. Preliminary, dimensionally accurate, 3D prostate phantom images have been produced.

14. SUBJECT TERMS
Ultrasound, imaging, diagnostic, elastography, 3D imaging, image processing

15. NUMBER OF PAGES
26

16. PRICE CODE

17. SECURITY CLASSIFICATION OF REPORT
Unclassified

18. SECURITY CLASSIFICATION OF THIS PAGE
Unclassified

19. SECURITY CLASSIFICATION OF ABSTRACT
Unclassified

20. LIMITATION OF ABSTRACT
Unlimited

Table of Contents

Cover.....	1
SF 298.....	2
Introduction.....	4
Body.....	5
Key Research Accomplishments.....	16
Reportable Outcomes.....	16
Conclusions.....	16
References.....	18
Appendix.....	19

INTRODUCTION

The American Cancer Society estimated that there would be approximately 230,110 new cases diagnosed and approximately 29,900 prostate cancer related deaths in 2004 [1]. Prostate cancer screening today generally uses the Prostate Specific Antigen (PSA) blood testing, free PSA testing and Digital Rectal Examination (DRE). When using a 'cutoff' of PSA > 4.0 ng/mL and an abnormal DRE, sensitivity, specificity and Positive Predictive Value (PPV) are 38%, 88% and 56% respectively [2]. When either an elevated PSA or an abnormal DRE are used, (in isolation – not in combination), sensitivity, specificity and PPV are even lower [2]. When the PSA is used there exists a significant gray area (4 - 10 ng/mL) in which cancers may be missed and yet the number of negative biopsies is large. Even though cancer detection sensitivity, specificity and PPV are improved by combining PSA and DRE [2, 3] the usefulness of DRE remains fundamentally limited due to its subjective nature. Additionally, DRE is practically limited to the detection of shallow (subcapsular) palpable abnormalities. Even systematic multi-core biopsy fails to detect clinically detectable cancers in up to 34% of men [4]. However, there is evidence that as additional biopsies cores are added, sensitivity improves [5]. This observation has resulted in an increase the number of cores taken during routine examination. Nevertheless, biopsy-based detection sensitivity remains less than ideal.

Thus, there is plenty of compelling clinical interest in finding improved methods for the early diagnosis of prostate cancer with improved sensitivity and specificity.

One recent example of progress in the field of prostate cancer detection involves an effort to automate the DRE examination. Savazyan recently described a system for 'mechanical imaging' of the prostate [6]. This system comprises a rectal probe that is instrumented with an array of pressure sensing strain gages and a 3D magnetic positioner device. In an *in vitro* trial [7], the new system correctly detected and located 100% of the nodules under examination. This compares with detection rates of 83% and 67% for an experienced urologist and a student respectively. Thus, a significant improvement over the conventional DRE examination has been demonstrated for the *in vitro* case. Another recent development is the observation that the sensitivity of an ultrasound examination can be improved by the use of a microbubble based contrast agents [4]. Frauscher's approach [4] involved the use of contrast agent enhanced Color Doppler that improved the detection of hypervascular regions associated cancer. Prostate cancer was detected by contrast agent assisted ultrasound in 23 of 24 patients known to have prostate cancer. (The method used for determining definitively which patients had cancer is not entirely clear in the article.) In comparison, conventional ultrasound detected cancer in 17 patients. The contrast agent assisted approach detected cancer in 8 patients with a negative systematic biopsy-based diagnosis. However, the cost of the contrast agent used in this study was \$65 per patient. This cost makes up approximately half of the cost of a conventional ultrasound examination and therefore represents a considerable impediment to its widespread acceptance. However, more recent publications [8, 9] (including one from Frauscher's group) cast doubt on the true extent of the improvement in diagnostic accuracy obtained by using contrast agents. Specifically, Halpern was unable to detect cancers in the inner gland and achieved a cancer detection sensitivity of only 42% [8].

BODY OF REPORT

The work conducted as part of this Army funded program can be considered as divided into the following key sections:

1. Research, design, development and prototype testing of a new transrectal ultrasound transducer, syringe pump and ultrasound instrumentation to facilitate a Synthetic Digital Rectal Examination (SDRE).
2. Research, development and prototype testing of techniques to enable quantitative (dimensionally accurate) 3D reconstructions of the prostate
3. Research, development and test of techniques to improve ultrasound image quality and to facilitate automated (or semi-automated) border detection of lesions
4. Small scale clinical test at the University of Virginia

Progress has been made in each of the first three tasks in the first year of the grant. It is intended that work relating to the fourth task will occur in the final year of the grant.

Progress with respect to the first three areas are related directly to the committed Statement of Work that was funded:

1. Design, specify, and have built, a high resolution transducer optimized for imaging elastic inhomogeneities, unsurpassed B-Mode image resolution and possessing integrated 3D capability.

A high frequency (8-14 MHz) transducer array has been designed and specified as committed. Vermon SA, Tours, France will make the transducer. We expect delivery in Q1 2005. Vermon has proven to be reliable in the past. The transducer will have two tracking arrays each with 32 elements and a central imaging array with 192 elements. The elements are spaced on a 0.2 mm pitch. This transducer should provide unsurpassed prostate imaging resolution. This transducer will provide the very best image data as a solid foundation for the successive work elements.

It should be noted that we have a lower frequency transrectal I-Beam transducer as an early prototype. This has enabled us to make progress on the other committed tasks.

The deliverable for this phase is an operable high resolution 3D-capable transducer array which we expect in Q1 2005. This is only a few months later than originally anticipated and since we have a 'fall back' position – i.e. using an older and slightly inferior device, we have not been delayed in making progress.

2. Develop and test a tissue elasticity imaging system.

As committed, we have assembled the apparatus to enable the new approach to transrectal ultrasound based strain imaging. We have procured a suitable versatile Harvard Instruments Syringe Pump, and necessary low cost supplies (tygon tubing, 60cc syringe, latex sheathes, small elastic bands). We have also assembled a number of prototype, custom prostate phantoms using techniques developed at in a colleague's laboratory (W. F. Walker) at the University of Virginia [10]. The ability to fabricate custom phantoms has been very useful in that it has allowed us to iterate on the design and determine optimal acrylamide (determines stiffness) and sephadex (determines gray scale backscatter) concentrations. We have successfully tested this system using an existing 8 MHz transrectal transducer connected to our Siemens Sequoia ultrasound machine. (It should be emphasized that practically all of the techniques planned can be migrated to other ultrasound systems if resource and contractual issues are addressed. The technology is 'portable'.)

The deliverable for this phase is a complete and validated (phantom) elasticity imaging system using the approach presented in the proposal. Significant progress has been made on this deliverable. Elasticity results with prototype phantoms have been obtained. Once we receive the new higher resolution transducer, it should be straightforward to upgrade our results using the new transducer to yield finer image resolution.

3. Apply image processing algorithms to acquired B-Mode and elasticity images to improve the quantification of detected elastic inhomogeneities

Early progress has been made with respect to this third aim. Specifically, we have applied the Speckle Reducing Anisotropic Diffusion (SRAD) [11] algorithm to our phantom ultrasound data. We have also made progress on extending SRAD to 3D. However, currently we believe that SRAD is better suited to 2D analysis on account of the computational expense of the algorithm. As commodity PC hardware improves, the time penalty of SRAD in 3D will become less burdensome. We have also obtained some early results using the well known Snakes algorithm [12]. This algorithm is well suited to ultrasound since it can be 'programmed' to avoid regions of dropout. Specifically, the 'rigidity' of the snake can be fine tuned according to the quality of the data. We have not made significant progress extending snakes in 2D to 3D. We have come to realize that this extension is more complex than we originally thought. Nevertheless, working with Scott Acton (partially funded collaborator) in Electrical and Computer Engineering, we anticipate making some progress in the remaining two years of the grant.

(The fourth item from the Statement of Work relates to a small scale clinical validation in collaboration with partially funded University of Virginia collaborator – Dr. Dan Theodorescu. This item of work will be actively addressed in the final year of the grant when the technology is fully developed and optimized.)

Summary Statement of work completed to date:

(Note: comprises significant part of work included as Appendix (a recent conference paper) plus some recent image processing results - i.e. the Appendix largely duplicates the content below)

Prostate Phantom

Experiments were performed using a laboratory-built acrylamide-based tissue mimicking phantom, prepared with a protocol based on the method by Negron [10]. The phantom comprises four components as shown in figure 1. The pea-sized inclusion is made of 17% (by weight) acrylamide gel to simulate a hard lesion. An egg-shaped surrounding is made of 5% acrylamide gel to mimic the soft prostate tissue. A round cavity on top of the egg-shaped surrounding with a diameter of 20mm to fit the transrectal transducer; and an outer body, also made of 5% acrylamide gel, enclosing all the other three structures. Sephadex was added to provide speckle both to the surrounding tissue and the inclusion, but not to the outside body. On the right of figure 1, the cavity is obscured in the image because the soft acrylamide-based outer body is not echogenic.

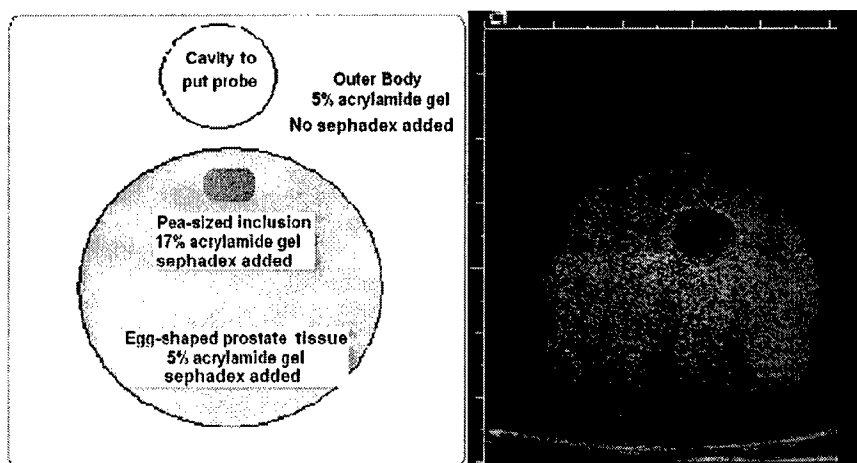


Figure 1. Left: Schematic of the purpose-built transrectal design of prostate phantom. Right: An ultrasound image was taken from above the outer body while the whole phantom was immersed in water. In this phantom, no sephadex was added in the inclusion in order to make it distinct from the surrounding tissue in the Bmode image. In the actually studied phantom (as shown in Figure 5), sephadex was added to both the inclusion and the surrounding tissue so that they both appear gray-white in B-mode images.

Imaging

A latex condom over the transrectal transducer was sealed in a conventional manner on the outside surface using elastic bands. The condom was controllably inflated with water using a syringe. The syringe volume of 60mL was chosen to provide sufficient displacement of the rectal wall for a measurable tissue strain signal while intrinsically avoiding the risk of over inflation of the condom. The maximum displacement at the top of the phantom was approximately 1.8 mm. This pressure and displacement are both well within safe limits for in vivo use. During the syringe inflation, a programmable syringe pump (PHD 2000, Harvard Apparatus, Holliston MA) was attached to the syringe to control the amount and rate of water injection. This permitted a continuous, uniform inflation process that enabled the image data set to be collected as one image sequence capture process. A Siemens Sequoia 512 scanner (Siemens Medical Solutions - originally Acuson, Mountain View, CA) was used in this study. Multiple demodulated (In-phase/Quadrature, I/Q) radio frequency beam-formed lines of acoustic data were acquired from the ultrasound scanner using a research interface employing an IQ data capture board. The data were then analyzed offline on a PC.

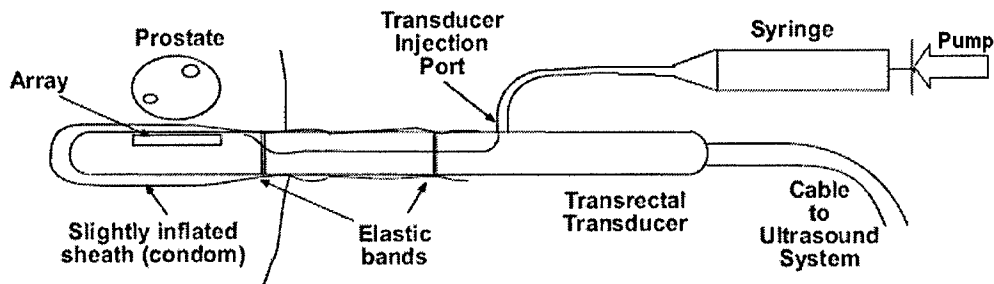


Figure 2. Prostate elasticity imaging schematic diagram. The transrectal ultrasound transducer is covered with a latex condom, which is secured to the transducer using elastic bands. An injection port is especially designed into the transducer for water injection. The condom is controllably inflated with water using a syringe. A programmable syringe pump is attached to the syringe to control the amount and rate of water injection. This provides a continuous pumping motion that enables the image data set to be collected as one image sequence capture process. (An optional pressure gage can be inserted in the fluid circuit. At steady state, the pressure in the condom is the same as would be measured by the gage in the fluid circuit.)

An 'I-Beam' design was implemented in the transrectal transducer. The I-Beam enables a freehand 3D imaging capability in that it has two 'Tracking' arrays orthogonally mounted on the two ends of the 'Imaging' array [13, 14]. When viewed from directly above the array, the imaging planes of the central and two tracking arrays form an 'I' shape – hence 'I-Beam'. When the transducer is translated or rotated in an elevational direction, multiple 2D image slices are acquired by the 'Imaging' array. The 'Tracking' arrays acquire multiple small image slices that are coplanar. These coplanar slices have the useful property that image frame to image frame motion tracking can be determined with high accuracy using image block matching techniques. This approach is compatible with current ultrasound biplane transrectal probes. This approach has been shown to yield a 2σ accuracy of 4.6% [13, 15]. The I-Beam approach is illustrated diagrammatically in Figure 3 and an image obtained by the transrectal I-Beam array is illustrated in Figure 4. I-Beam is also uniquely matched to this particular application for the following reasons:

1. Since the transrectal probe is long and thin, it is preferable to place the position and orientation means of determination near the transducer tip where the acoustic array is positioned. If the positioning means is placed relatively far away near the handle, then there is significant scope for numerical ill-conditioning. (Small angular errors result in significant positional errors at the tip.)
2. I-Beam measures relative motion. If tissue moves in a global sense (with respect to a fixed axis origin) during transducer motion, then by using only relative measures of motion, no gross dimensional error results. If tissue motion occurs when a fixed reference origin is used (e.g. if using a magnetic positioner [6] or an articulated arm [16]) then a dimensional error will occur in the resulting 3D reconstruction.

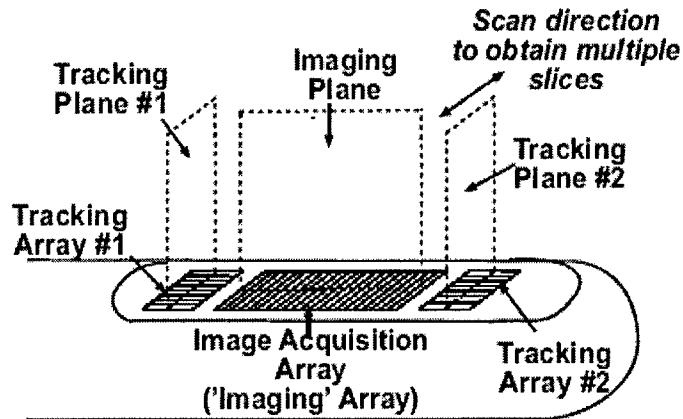


Figure 3. Architecture of 'I-Beam' transrectal transducer, i.e., an integrated transducer with an 'Imaging' array and two orthogonally mounted 'Tracking' arrays.

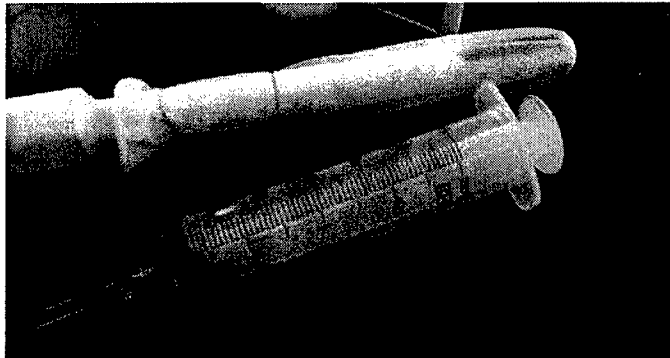


Figure 4. Actual 'I-Beam' transrectal transducer inside latex sheath. Syringe and tygon tubing connected. Water is injected into the sheath via a special purpose channel through the transducer that expels water near the tip of the transducer.

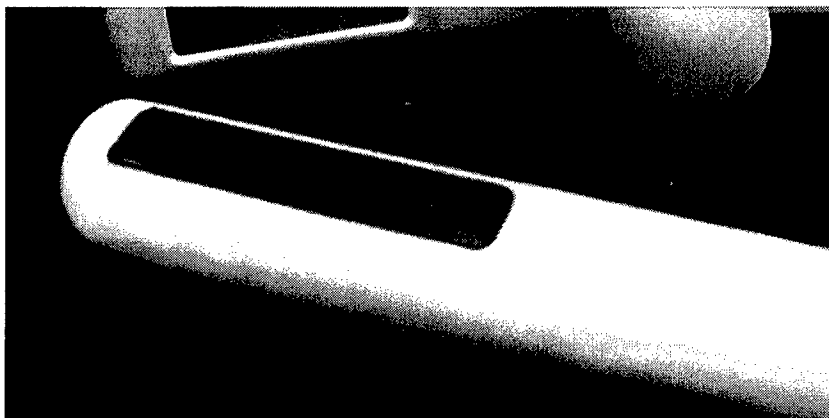


Figure 5 Close up of I-Beam transducer showing tracking arrays as revealed by different shape of acoustic lens. Note that these images are of the early prototype. The higher resolution transducer is in progress.

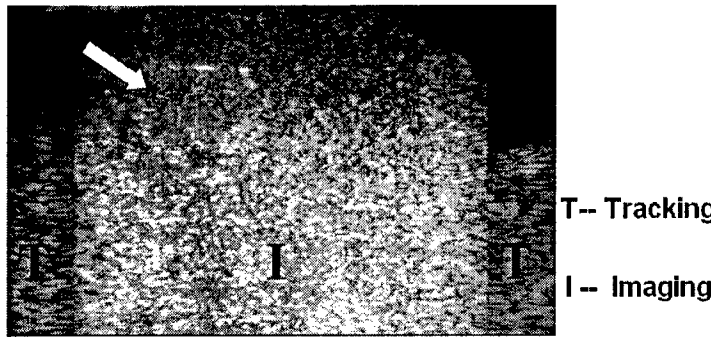


Figure 6. The image acquired with the I-Beam transrectal transducer from the prostate-mimicking phantom, showing the layout of image planes formed by 'Tracking' arrays and 'Imaging' array. The arrow is pointing to a hard inclusion simulating a lesion in the prostate. As in real prostate B-mode ultrasound images, the lesion is hard to identify in this regular B-mode image. (The Tracking data appears dimmer in this image because aperture size related gain compensation was not employed when the software running the transducer was developed. Making such compensation would have required additional resources from Siemens engineering staff. This issue could be rectified if the technique is fully developed.)

As pressure due to the water injection is applied to the phantom, deformation is generated in both the lesion and the surrounding tissue. Deformations of lesion and tissue can be distinguished because the strains in each are different due to their different moduli of elasticity. To determine the deformation, the displacement coefficients between two image frames were calculated on the I/Q data using cross-correlation. The lag index corresponding to the greatest cross-correlation coefficient, i.e., the best match was calculated for each search window, in this case with a size of four RF cycles in axial dimension. Subsample precision was obtained by using quadratic interpolation around the cross-correlation best match. Repeating this process throughout the I/Q data of the image frame created a displacement map between two frames. The strain image was obtained by spatial differentiation, in the range dimension, of the displacement map.

In the elevation direction, a block matching approach based upon the minimum sum of absolute differences (MSAD) algorithm was performed on the I-Beam 'Tracking' data. A trackable (i.e. containing fully developed speckle) of the image was chosen in both tracking image planes, and five matching blocks evenly spaced long the depth direction of the image were selected in each tracking image plane. Each matching block contained 32×32 pixels. These image blocks contain approximately two to four individual speckles. Displacement was found to be larger in the deeper portion than in the shallower portion, indicating that the transducer was rotated by a small angle between measurements. In the measurements, the 2D acquisitions were sampled with a frame interval no greater than 2mm, and the rotation angle increments were less than 3 degrees, in order to ensure that the elevational motion could be accurately tracked. Once the elevational motion of these blocks was calculated, the acquired image slices were interpolated on to a regular 3D grid in Matlab, enabling 3D volumes to be rendered.

Figure 7 illustrates the lesion detection process. The displacement map was calculated on the I/Q data with a cross-correlation operation followed by quadratic interpolation. The lesion was detected based on the amplitude of the strain image. A threshold technique, after image filtering to decrease noise, was applied on the strain image using a threshold value of 1.4%. Low strain Low strain regions (i.e. resulting from high stiffness) were rendered using a translucent green mask, superimposed onto the B-mode image so as to maintain the higher spatial resolution of the original B-Mode data while simultaneously highlighting elastically anomalous tissue.

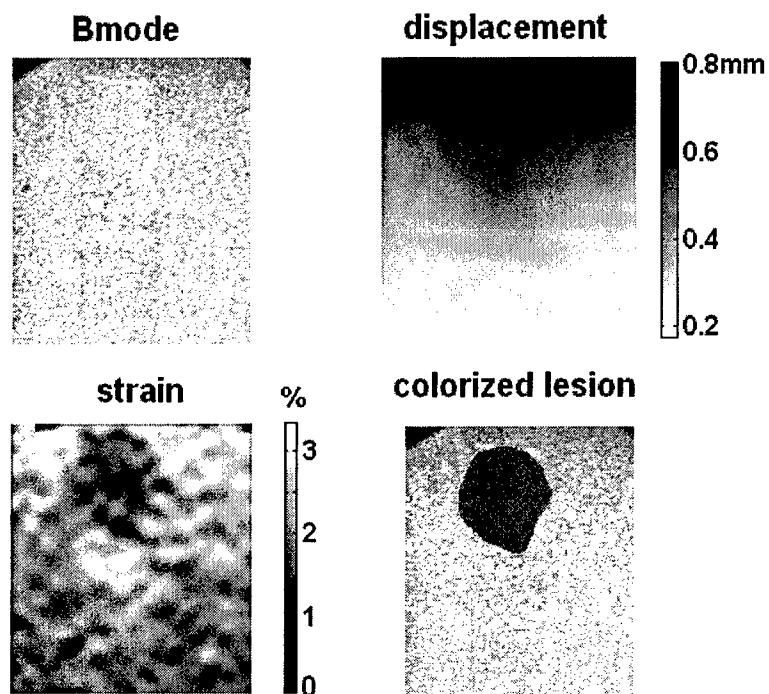


Figure 7. Lesion detection. The lesion is barely identifiable in the original B-mode image, but its visibility is significantly enhanced in the displacement map, strain image and the colorized lesion image. The displacement map and strain image are shorter than the original B-mode image because a stripe with a height of a search window height was cut off on either end.

I-Beam 3D imaging

In addition to generating images of elasticity, we have also tested the ability of the prototype I-Beam transducer to obtain 3D reconstructions of the phantom lesion.

Figure 8 illustrates some sample tracking image data sets. Notice the easily detectable rightward shift between the two images. Our motion estimation algorithm – based on Minimum Sum of Absolute Differences (MSAD) with parabolic curve fitting around the minimum to resolve motion to subpixel resolution. The well formed speckle lends itself to good tracking.

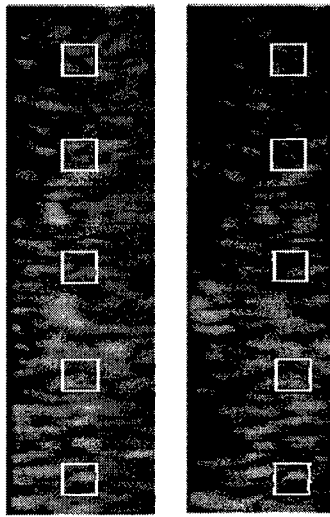


Figure 8. Image frame to frame motion detected on the image planes formed by the tracking arrays using a MSAD image block matching technique. The highlighted blocks show the transverse displacements between the two coplanar frames. For imaging arrays, these transverse displacements are in the elevational direction.

Using the same prostate phantom as described above, an I-Beam sweep was performed and arbitrary slices and a 3D surface rendering reconstructed. Figure 9 shows image planes rendered in three dimensions. Figure 10 shows the 3D surface rendering of the lesion, side by side with the photograph of the actual inclusion. The volumes calculated from three independent ultrasound measurements for this lesion were 258, 267 and 274 μl corresponding to a mean value of 266 μl and a Standard Deviation of 8 μl . The volume of the actual inclusion was measured to be approximately 300 μl using Archimede's principle in a graduated cylinder. We estimate the precision and accuracy of our measurement of the lesion of the volume to be $\pm 30 \mu\text{l}$ (10%). Thus, the lack of a precise and accurate method for determining exact actual volume limits our ability to precisely and accurately quantify the accuracy of our reconstruction. Nevertheless, this early result is encouraging when taking account of the fact that errors in all three orthogonal directions can compound to degrade final volumetric accuracy. Furthermore, in previous studies using a transducer with similar acoustic characteristics to the one used here, we obtained a linear 2σ accuracy of 4.6% in the reconstructed (transducer elevation) dimension [13].

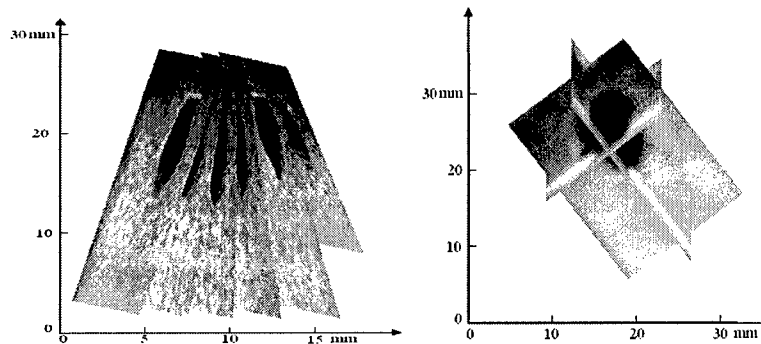


Figure 9. 3D reconstruction of the lesion. Left: The multiple 2D image slices acquired were rendered in three dimensions. The slight obliqueness of these image slices indicates a rotational sweep in the acquisition process. The lesion was detected and shown in black. Right: An orthogonal plane view of the identified lesion. The image was blurred due to interpolation and smoothing on the sparse image samples.

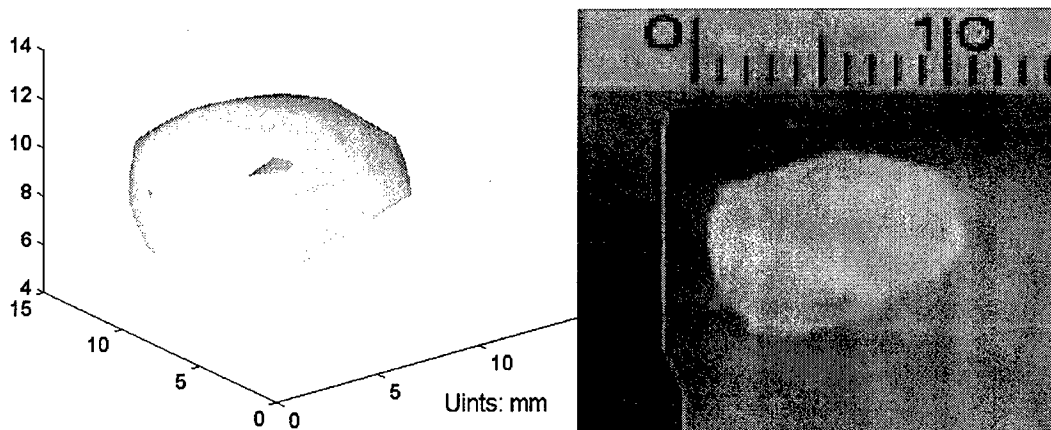


Figure 10. Left: The prostate lesion detected from the ultrasound images. The lesion was segmented from the surrounding tissue and its 3D surface was rendered. The volume calculated for this reconstructed lesion is $266 \pm 8 \mu\text{l}$. Right: a photograph of the real inclusion. Its volume is $300 \pm 30 \mu\text{l}$. Therefore the error is approximately 11%. (The uncertainty in the accuracy is limited more by the uncertainty in the 'actual' measurement than in the inaccuracy of the I-Beam method.)

Image Processing

We have also investigated the utility of the Speckle Reducing Anisotropic Diffusion (SRAD) [11] algorithm developed by our colleagues Yu and Acton in the Electrical and Computer Engineering Department at the University of Virginia.

Figure 11 illustrates early results using ultrasound phantom data. It is readily evident that SRAD is able to reduce speckle content in the image and yet maintain excellent border definition. Most speckle reduction algorithms degrade border definition. However, SRAD avoids this by using a different diffusion parameter in the vicinity of an edge.

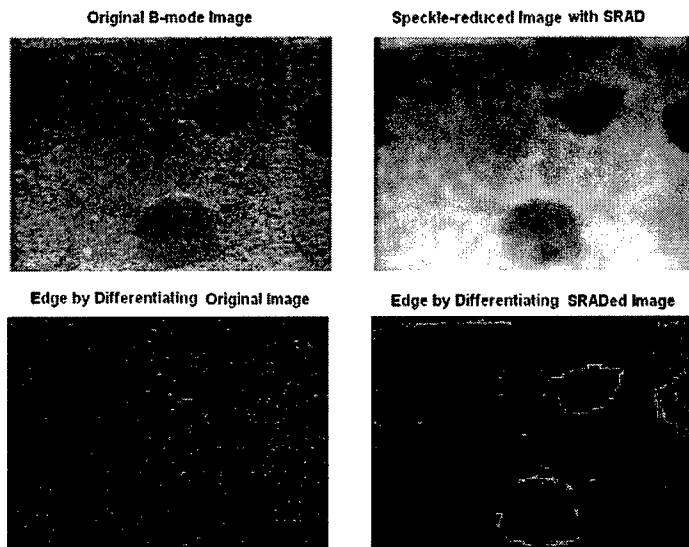


Figure 11 Top left: Original raw, speckle phantom image

Top right: Same image as at left after application of Speckle Reducing Anisotropic Diffusion (SRAD) [11]. Note the reduction in speckle without a loss in lesion border definition.
Bottom left: Gradient (difference) applied to original image – correct borders undetectable.
Bottom Right: Gradient (difference) applied to SRAD image – correct borders are easily detectable.

Figure 12 shows a second sequence of images that demonstrate the contribution of SRAD as a preprocessing stage when using 'active contours' or 'snakes'. Figure 12b shows the result of SRAD on Figure 12a which is ultrasound data acquired from an ultrasound prostate phantom. After SRAD, the prostate boundary is clarified and in fact, enhanced. To quantify the improvement in segmentation allowed by SRAD we utilize a well known image segmentation tool, the active contour [17]. An active contour is a flexible contour that automatically delineates objects. A contour is initially placed near the object boundary, either manually or automatically. Starting from the initial location, the contour gradually deforms in order to locate the object boundary. This deformation process, executed through iterative computations, is known as the contour evolution. Contour evolution is complete once the differential changes in position converge to zero. This final contour delineates the desired object.

To alleviate dependence of the final contour on initial contour location, we utilize another well known image processing tool, gradient vector flow (GVF) [12]. GVF diffuses edge information away from the object boundary. Thus, an active contour initialized away from the desired boundary is able to sense the boundary and delineate the object.

Using an active contour equipped with GVF, we segmented ten ultrasound images of a prostate. We first segmented all ten of the original, unprocessed images. We then processed each image with SRAD and repeated the segmentation. Figures 12c and 12d show the results of active contour segmentation of the unprocessed and processed image, respectively. The same contour initialization was utilized in both the unprocessed and processed images, shown as white circles.

To quantify segmentation error, we compare the segmented prostate boundary with manually derived prostate contours. Two types of error measures between the automatic and manual segmentation have been considered: the root mean squared error (RMSE) and the Pratt figure of merit (FOM)[18]. RMSE measures the distance between two contour points averaged over the entire contour. The FOM is a number between 0 and 1 that specifies how close the segmented contour is near the actual edge, which in this case is the manually traced prostate boundary. The FOM scales the merit segmentation from 0 to 1; 1 being the highest merit for a perfect match. Table 1 specifies the results of segmentation quantified by RMSE and FOM.

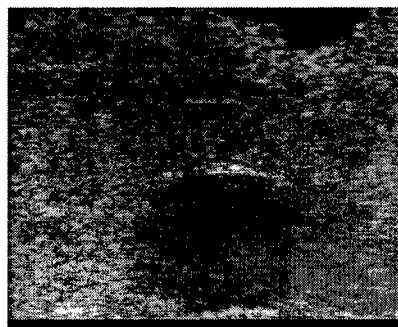


Figure 12a: Unprocessed ultrasound image of prostate.



Figure 12b: SRAD of figure 12a prostate image.



Figure 12c: Segmentation of unprocessed ultrasound image of prostate.

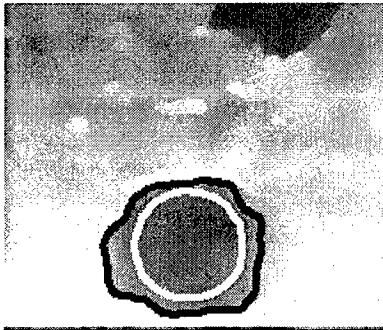


Figure 12d: Segmentation of SRAD-processed ultrasound image of prostate.

image #	RMSE (pixels)		Pratt FOM	
	Unprocessed	Processed	Unprocessed	Processed
100	15.4361	3.3679	0.2412	0.5772
101	15.2522	2.7693	0.3331	0.6714
102	15.6319	2.9528	0.2949	0.6501
103	13.7116	2.2031	0.2153	0.7183
104	24.6591	3.338	0.2188	0.6254
105	18.4705	3.9416	0.2801	0.5452
106	19.9994	4.7844	0.1976	0.4643
107	15.3547	5.2576	0.2282	0.4648
108	17.8084	5.5042	0.2137	0.3988
109	15.9488	4.7093	0.244	0.4208
110	18.4273	5.1253	0.1714	0.4274

Table 1: RMSE and Pratt FOM for unprocessed (before SRAD) and processed (after SRAD) ultrasound prostate images.

KEY RESEARCH ACCOMPLISHMENTS

- We have assembled the key components for our Synthetic Digital Rectal Examination – comprising modified ultrasound transducer, later sheath, tubing, syringe and syringe pump, several laboratory-made realistic rectal examination-based ultrasound prostate phantoms and required driving instrumentation (ultrasound scanner with required software). The current apparatus temporarily uses a lower resolution transducer (up to 8 MHz). We expect to replace this in the next four months with a 14 MHz transducer that will provide practically unsurpassed prostate ultrasound imaging. In addition to have the ability to test for elastic inhomogeneities, the system has a versatile, and easy-to-use 3D acquisition capability.
- We have verified the efficacy of our approach for detecting hard lesions in a prostate tissue phantom
- We have verified the accuracy of our approach to quantify 3D volumes in a prostate tissue phantom

REPORTABLE OUTCOMES

We have very recently presented our first conference paper on this work. It was a presentation at the SPIE Medical Imaging meeting in February 2005 in San Diego. We also anticipate submitting one or more papers to the IEEE International Ultrasonics Symposium in 2005. These two conferences are the best venues for technical contributions in medical diagnostic ultrasound. We also plan to publish components of our work in archival journals. For reference, the SPIE proceedings are sometimes counted as archival and full length (8 pages in our case) papers become part of the written and electronically searchable (INSPEC) record.

CONCLUSIONS

Our prostate imaging approach combines using an I-Beam transducer enabling easy-to-use, accurate and versatile 3D capability with elasticity imaging for detecting inhomogeneities of the type normally detected in DRE. We have tested out system on phantoms to-date. Testing on humans requires further development of the instrumentation and obtaining the requisite human

protection clearance both internal to the University of Virginia and from the US Army.

The prostate strain imaging performed here using a slightly inflated sheath over the transrectal transducer significantly enhanced tumor visibility (a hard inclusion in the phantom). The lesion was nearly invisible in the regular B-mode image. The I-Beam transducer enabled reconstruction of discrete 2D image acquisitions into regular 3D grid space, and thus the tumor was rendered in 3D. The volume calculated for this tumor had an error of approximately 11% compared to the actual (independently determined) volume.

So what? Section

Our approach shows promise as a valuable approach for improving prostate cancer detection since we believe that it will be more sensitive and more specific than current methods based on using DRE. Even when DRE is combined with PSA, current levels of sensitivity and specificity obtained using these conventional techniques are grossly inadequate.

REFERENCES

1. American Cancer Society, *Prostate Cancer Statistics from www.cancer.org*. 2003.
2. Crawford, E., et al., *Efficiency of Prostate-Specific Antigen and Digital Rectal Examination in Screening, Using 4.0 ng/mL and Age Specific Reference Range as a Cutoff for Abnormal Values*. *The Prostate*, 1999. **38**: p. 296-302.
3. Toubert, M., et al., *Screening for cancer of the prostate using prostate-specific antigen*. *Presse Medicale*, 1990. **19**(24): p. 1139-1142.
4. Frauscher, F., et al., *Detection of Prostate Cancer with a Microbubble Ultrasound Contrast Agent*. *The Lancet*, 2001. **357**: p. 1849-1850.
5. Taylor, J., et al., *Increasing the number of core samples taken at prostate needle biopsy enhances the detection of clinically significant prostate cancer*. *Urology*, 2002. **60**(5): p. 841-845.
6. Sarvazyan, A., *Mechanical imaging: a new technology for medical diagnostics*. *Journal of Medical Informatics*, 1998. **49**(2): p. 195-216.
7. Weiss, R., et al., *In vitro trial of the pilot prototype of the prostate mechanical imaging system*. *Urology*, 2001. **58**(6): p. 1059-1063.
8. Halpern, E., et al., *Contrast-enhanced US of the Prostate with SonoZoid: Comparison with Whole-Mount Prostatectomy Specimens in 12 Patients*. *Radiology*, 2002. **222**: p. 361-366.
9. Clements, R., *The Role of Transrectal Ultrasound in Diagnosing Prostate Cancer*. *Current Urology Reports*, 2002. **3**: p. 194-200.
10. Negron, L., et al., *Development and characterization of a vitreous mimicking material for radiation force imaging*. *IEEE Transactions Ultrasonics, Ferroelectrics and Frequency Control*, 2002. **49**(11): p. 1543-1551.
11. Yu, Y. and S. Acton, *Snakes reducing anisotropic diffusion*. *IEEE Transactions on Image Processing*, 2002. **11**: p. 1260-1270.
12. Xu, C. and J. Prince, *Snakes, Shapes and Gradient Vector Flow*. *IEEE Trans. Image Processing*, 1998. **7**(3): p. 359-369.
13. Hossack, J.A., et al., *Quantitative 3D Diagnostic Ultrasound Imaging Using a Modified Transducer Array and an Automated Image Tracking Technique*. *IEEE Transactions on Ultrasonics Ferroelectrics & Frequency Control*, 2002. **49**(8): p. 1029-1038.
14. Hossack, J., T. Sumanaweera, and S. Napel. *Quantitative 3D Ultrasound Imaging Using an Automated Image Tracking Technique*. in *IEEE Ultrasonics Symposium*. 2000: IEEE.
15. Napel, S., et al., *Carotid Disease: Automated Analysis with Cardiac-gated Three-dimensional US Technique and Preliminary Results*. *Radiology*, 2002. **222**(2): p. 560-563.
16. Prager RW, R.R., Gee AH, Berman L, *Rapid calibration for 3-D freehand ultrasound*. *Ultrasound Med Biol*, 1998. **24**(6): p. 855-69.
17. Kass, M., A. Witkin, and D. Terzopoulos, *Snakes: Active contour models*. *International Journal of Computer Vision*, 1987: p. 321-331.
18. Pratt, W., *Digital image processing*. 1981, New York: John Wiley.

Appendix: (Presented at SPIE Medical Imaging, February 2005)
Combined Elasticity and 3D Imaging of the Prostate

Yinbo Li and John A. Hossack

Biomedical Engineering Department, University of Virginia, Charlottesville, VA 22908-0759

ABSTRACT

A method is described for repeatably assessing elasticity and 3D extent of suspected prostate cancers. Elasticity is measured by controlled water inflation of a sheath placed over a modified transrectal ultrasound transducer. The benefit of using fluid inflation is that it should be possible to make repeatable, accurate, measurements of elasticity that are of interest in the serial assessment of prostate cancer progression or remission. The second aspect of the work uses auxiliary tracking arrays placed at each end of the central imaging array that allow the transducer to be rotated while simultaneously collected 'tracking' information thus allowing the position of successive image planes to be located with approximately 8% volumetric accuracy in 3D space. In this way, we present a technique for quantifying volumetric extent of suspected cancer in addition to making measures of elastic anomalies.

1. INTRODUCTION

Prostate cancer is the second most prevalent malignant cancer in North American men. Each year there are approximated 220,000 new cases and 28,900 deaths [1]. Current cancer screening techniques exhibit disappointing sensitivity and specificity. In this work we describe a 'Synthetic Digital Rectal Examination' using a technique we conceived independently but which has recently been described by Alam [2]. We prefer this technique since we believe that it may yield an approach for providing repeatable measurements so that serial analyses can be performed in the clinical setting. In many clinical situations it is desirable to assess the progress or response to treatment of a palpable lesion. However, the digital rectal examination (DRE) is subject to both intra-observer and inter-observer variation. Additionally, since ultrasound elastographic techniques can detect displacements of the order of a small fraction of an ultrasound wavelength (i.e. a small number of microns), ultrasound elastography ought to be more intrinsically sensitive [3-6]. We also believe that with the correct instrumentation the time penalty for using this technique as opposed to freehand scanning will be insignificant as compared to patient and transducer preparation time. For example, the sheath can be inflated and deflated controllably by a syringe pump in a matter of a few seconds.

The 3D portion of this work is enabled using an 'I-Beam' transducer [7]. This approach allows the transducer to be rotated gradually while 2D image position and orientation information is simultaneously acquired. We have acquired both strain imaging and 3D image data using a laboratory-built phantom and report early results. Our preferred strain display approach is to colorize the underlying B-Mode image data according to measured strain and in this way maintain the high spatial resolution of the original B-Mode data. In 3D reconstructions of the lesions in the prostate phantom we have achieved dimensional accuracy of approximately 5%. This accuracy is broadly within that achievable using other 3D positioning techniques and is similar to the accuracy that can be realistically claimed in the ultrasound axial beam direction after taking account of speed of realistic sound variations.

Static elasticity imaging using ultrasound has been intensively studied for many years. This technique requires capturing multiple frames of data during deformation in tissue. The deformation is caused by an external force that is usually applied by gently pushing the transducer into the subject's tissue. Phase sensitive correlation-based algorithms estimate the tissue displacements between frames to create displacement maps. Strain images are derived from displacement data via differentiation with respect to axial range [3-6].

2. METHODS

2.1 Prostate Phantom

The experiments were performed on a laboratory-built acrylamide-based tissue mimicking phantom, prepared with a protocol based on the method by Negron [8]. The phantom comprises four components as shown in figure 1. The pea-sized inclusion is made of 17% (by weight) acrylamide gel to simulate a hard lesion. An egg-shaped surrounding is made of 5% acrylamide gel to mimic the soft prostate tissue. A round cavity on top of the egg-shaped surrounding with a diameter of 20mm to fit the transrectal transducer; and an outer body, also made of 5% acrylamide gel, enclosing all the other three structures. Sephadex was added to provide speckle both to the surrounding tissue and the inclusion, but not to the outside body. On the right of figure 1, the cavity is obscured in the image because the soft acrylamide-based outer body is not echogenic.

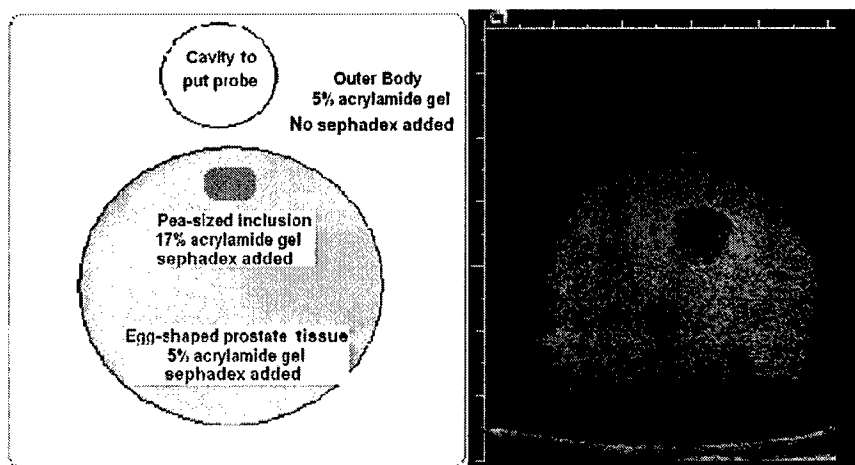


Figure 1. Left: Schematic of the purpose-built transrectal design of prostate phantom. Right: An ultrasound image was taken from above the outer body while the whole phantom was immersed in water. In this phantom, no sephadex was added in the inclusion in order to make it distinct from the surrounding tissue in the Bmode image. In the actually studied phantom (as shown in Figure 5), sephadex was added to both the inclusion and the surrounding tissue so that they both appear gray-white in B-mode images.

2.2 Imaging

A latex condom over the transrectal transducer was sealed in a conventional manner on the outside surface using elastic bands. The condom was controllably inflated with water using a syringe. The syringe volume of 60mL was chosen to provide sufficient displacement of the rectal wall for a measurable tissue strain signal while intrinsically avoiding the risk of over inflation of the condom. The maximum displacement at the top of the phantom was approximately 1.8 mm. This pressure and displacement are both well within safe limits for in vivo use. During the syringe inflation, a programmable syringe pump (PHD 2000, Harvard Apparatus, Holliston MA) was attached to the syringe to control the amount and rate of water injection. This permitted a continuous, uniform inflation process that enabled the image data set to be collected as one image sequence capture process. A Siemens Sequoia 512 scanner (Siemens Medical Solutions - originally Acuson, Mountain View, CA) was used in this study. Multiple demodulated (In-phase/Quadrature, I/Q) radio frequency beam-formed lines of acoustic data were acquired from the ultrasound scanner using a research interface employing an IQ data capture board. The data were then analyzed offline on a PC.

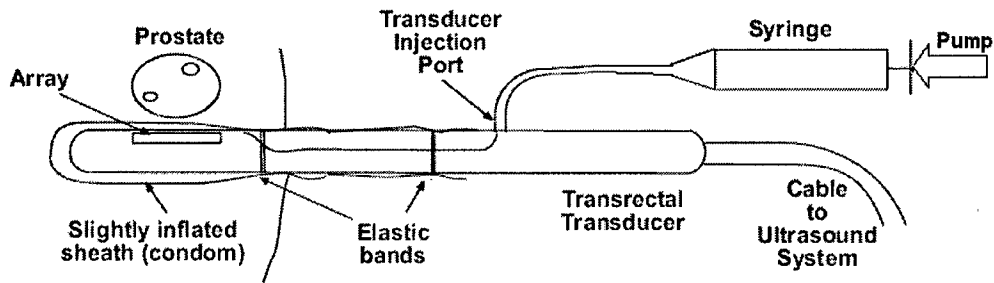


Figure 2. Prostate elasticity imaging schematic diagram. The transrectal ultrasound transducer is covered with a latex condom, which is secured to the transducer using elastic bands. An injection port is especially designed into the transducer for water injection. The condom is controllably inflated with water using a syringe. A programmable syringe pump is attached to the syringe to control the amount and rate of water injection. This provides a continuous pumping motion that enables the image data set to be collected as one image sequence capture process. (An optional pressure gage can be inserted in the fluid circuit. At steady state, the pressure in the condom is the same as would be measured by the gage in the fluid circuit.)

An 'I-Beam' design was implemented in the transrectal transducer. The I-Beam enables a freehand 3D imaging capability in that it has two 'Tracking' arrays orthogonally mounted on the two ends of the 'Imaging' array [7, 9]. When the transducer is translated or rotated in an elevational direction, multiple 2D image slices are acquired by the 'Imaging' array. The 'Tracking' arrays acquire multiple small image slices that are coplanar. These coplanar slices have the useful property that image frame to image frame motion tracking can be determined with high accuracy using image block matching techniques. This approach is compatible with current ultrasound biplane transrectal probes. This approach has been shown to yield a 2σ accuracy of 4.6% [7, 10]. The I-Beam approach is illustrated diagrammatically in Figure 3 and an image obtained by the transrectal I-Beam array is illustrated in Figure 4. I-Beam is also uniquely matched to this particular application for the following reasons:

1. Since the transrectal probe is long and thin, it is preferable to place the position and orientation means of determination near the transducer tip where the acoustic array is positioned. If the positioning means is placed relatively far away near the handle, then there is significant scope for numerical ill-conditioning. (Small angular errors result in significant positional errors at the tip.)
3. I-Beam measures relative motion. If tissue moves in a global sense (with respect to a fixed axis origin) during transducer motion, then by using only relative measures of motion, no gross dimensional error results. If tissue motion occurs when a fixed reference origin is used (e.g. if using a magnetic positioner [11] or an articulated arm [12]) then a dimensional error will occur in the resulting 3D reconstruction.

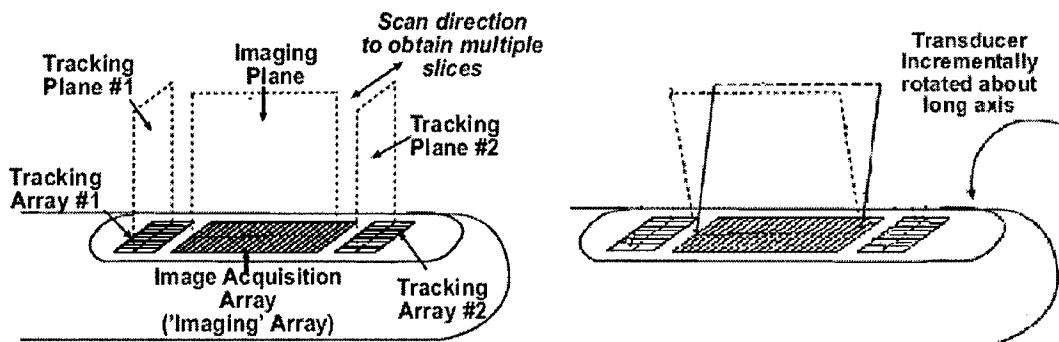


Figure 3. Left: Architecture of 'I-Beam' transrectal transducer, i.e., an integrated transducer with an 'Imaging' array and two orthogonally mounted 'Tracking' arrays. Right: The incremental rotation in the acquisition process. The transducer was rotated by a few degrees between acquisitions of successive 2D image slices so as to obtain multiple 2D image data sets with known inter-plane spacing in 3D space.

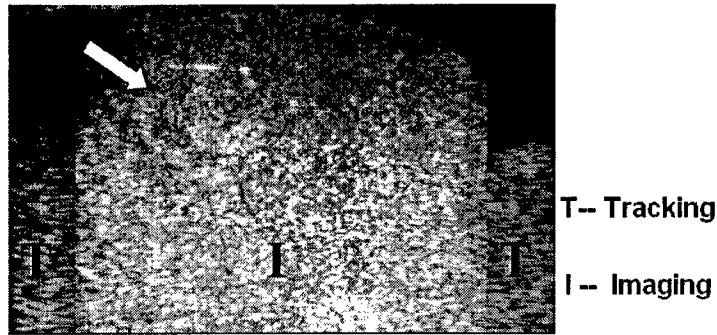


Figure 4. The image acquired with the I-Beam transrectal transducer from the prostate-mimicking phantom, showing the layout of image planes formed by 'Tracking' arrays and 'Imaging' array. The arrow is pointing to a hard inclusion simulating a lesion in the prostate. As in real prostate B-mode ultrasound images, the lesion is hard to identify in this regular B-mode image. (The Tracking data appears dimmer in this image because aperture size related gain compensation was not employed when the software running the transducer was developed. Making such compensation would have required additional resources from Siemens engineering staff. This issue could be rectified if the technique is fully developed.)

As pressure due to the water injection is applied to the phantom, deformation is generated in both the lesion and the surrounding tissue. Deformations of lesion and tissue can be distinguished because the strains in each are different due to their different moduli of elasticity. To determine the deformation, the displacement coefficients between two image frames were calculated on the I/Q data using cross-correlation. The lag index corresponding to the greatest cross-correlation coefficient, i.e., the best match was calculated for each search window, in this case with a size of four RF cycles in axial dimension. Subsample precision was obtained by using quadratic interpolation around the cross-correlation best match. Repeating this process throughout the I/Q data of the image frame created a displacement map between two frames. The strain image was obtained by spatial differentiation, in the range dimension, of the displacement map.

In the elevation direction, a block matching approach based upon the minimum sum of absolute differences (MSAD) algorithm was performed on the I-Beam 'Tracking' data. A trackable (i.e. containing fully developed speckle) of the image was chosen in both tracking image planes, and five matching blocks evenly spaced along the depth direction of the image were selected in each tracking image plane. Each matching block contained 32×32 pixels. These image blocks contain approximately two to four individual speckles. Displacement was found to be larger in the deeper portion than in the shallower portion, indicating that the transducer was rotated by a small angle between measurements. In the measurements, the 2D acquisitions were sampled with a frame interval no greater than 2mm, and the rotation angle increments were less than 3 degrees, in order to ensure that the elevational motion could be accurately tracked. Once the elevational motion of these blocks was calculated, the acquired image slices were interpolated on to a regular 3D grid in Matlab, enabling 3D volumes to be rendered.

3. RESULTS

Figure 6 illustrates the lesion detection process. The displacement map was calculated on the I/Q data with a cross-correlation operation followed by quadratic interpolation. The lesion was detected based on the amplitude of the strain image. A threshold technique, after image filtering to decrease noise, was applied on the strain image using a threshold value of 1.4%. Low strain Low strain regions (i.e. resulting from high stiffness) were rendered using a translucent green mask, superimposed onto the B-mode image so as to maintain the higher spatial resolution of the original B-Mode data while simultaneously highlighting elastically anomalous tissue.

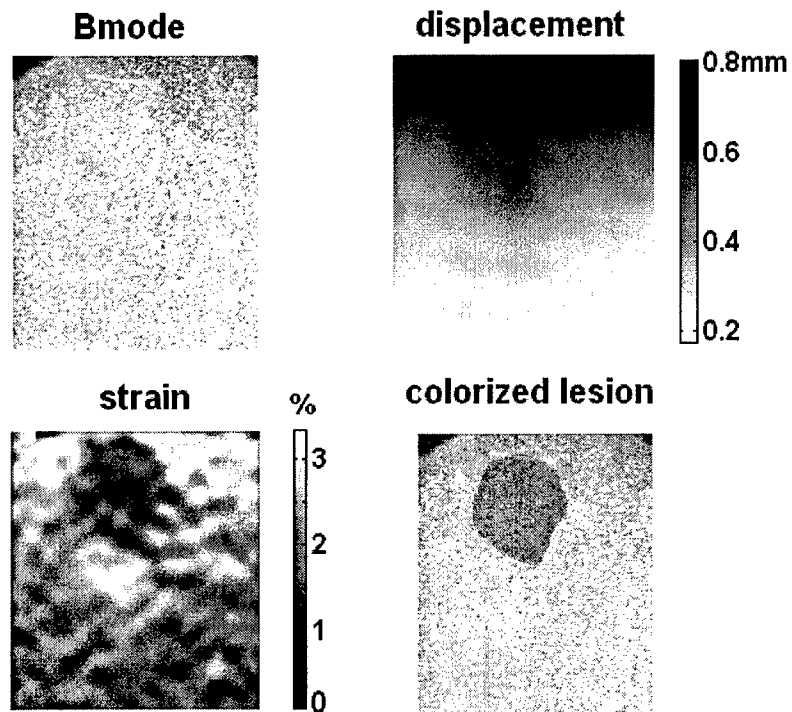


Figure 6. Lesion detection. The lesion is barely identifiable in the original B-mode image, but its visibility is significantly enhanced in the displacement map, strain image and the colorized lesion image. The displacement map and strain image are shorter than the original B-mode image because a stripe with a height of a search window height was cut off on either end.

Figure 7 shows elevational motion detection by tracking the image planes formed by the tracking arrays.

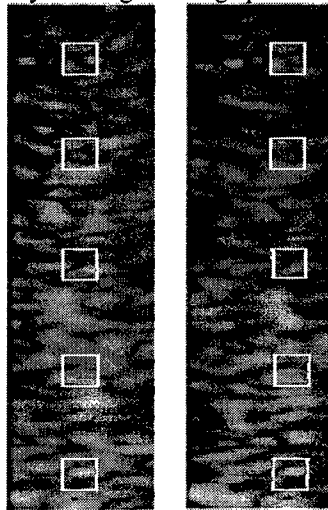


Figure 7. Image frame to frame motion detected on the image planes formed by the tracking arrays using a MSAD image block matching technique. The highlighted blocks show the transverse displacements between the two coplanar frames. For imaging arrays, these transverse displacements are in the elevational direction.

Arbitrary slices and surface rendering were performed based on the three-dimensional reconstruction. Figure 8 shows image planes rendered in three dimensions. Figure 9 shows the 3D surface rendering of the lesion, side by side with the photograph of the actual inclusion. The volumes calculated from three independent ultrasound measurements for this lesion were 258, 267 and 274 μl corresponding to a mean value of 266 μl and a Standard Deviation of 8 μl . The volume of the actual inclusion was measured to be approximately 300 μl using Archimede's principle in a graduated cylinder. We estimate the precision and accuracy of our measurement of the lesion of the volume to be $\pm 30 \mu\text{l}$ (10%). Thus, the lack of a precise and accurate method for determining exact actual volume limits our ability to precisely and accurately quantify the accuracy of our reconstruction. Nevertheless, this early result is encouraging when taking account of the fact that errors in all three orthogonal directions can compound to degrade final volumetric accuracy. Furthermore, in previous studies using a transducer with similar acoustic characteristics to the one used here, we obtained a linear 2σ accuracy of 4.6% in the reconstructed (transducer elevation) dimension [7].

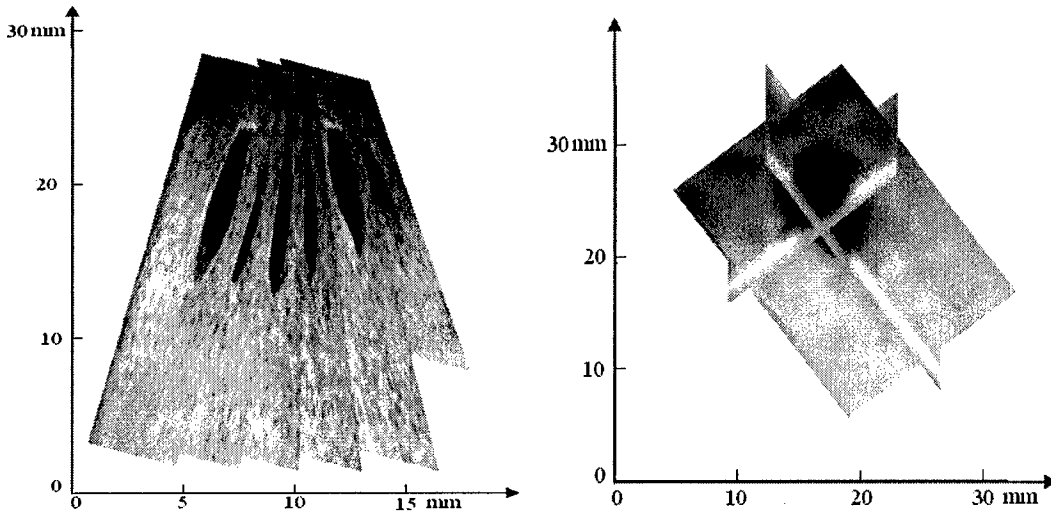


Figure 8. 3D reconstruction of the lesion. Left: The multiple 2D image slices acquired were rendered in three dimensions. The slight obliqueness of these image slices indicates a rotational sweep in the acquisition process. The lesion was detected and shown in black. Right: An orthogonal plane view of the identified lesion. The image was blurred due to interpolation and smoothing on the sparse image samples.

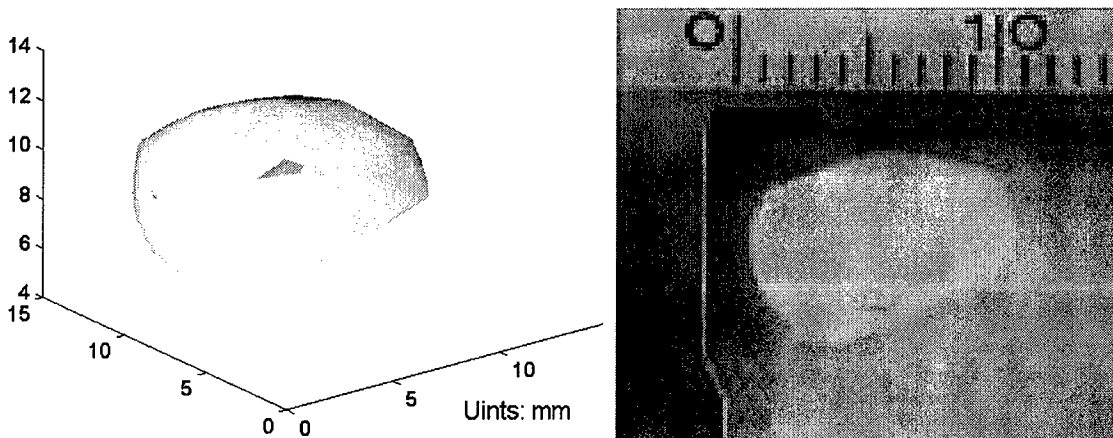


Figure 9. Left: The prostate lesion detected from the ultrasound images. The lesion was segmented from the surrounding tissue and its 3D surface was rendered. The volume calculated for this reconstructed lesion is $266 \pm 8 \mu\text{l}$. Right: a photograph of the real inclusion. Its volume is $300 \pm 30 \mu\text{l}$. Therefore the error is about 11%.

4. DISCUSSION

The elasticity imaging of prostate using an inflated sheath described here is advantageous because of three reasons. Firstly, fewer problems resulting from image decorrelation were induced by gross transducer motion since the inflation process is well controlled. Secondly, the intra-sheath pressure was controlled and indirectly monitored by the syringe pump. Thus, the measurement is repeatable since the amount of applied pressure / displacement inside the rectum is controlled and known, and thus the repeatability in the elasticity imaging is improved. Thirdly, by using the gentle pressure of the water filled condom, a far more uniform pressure distribution was achieved in the simulated rectum than can be obtained by simply pressing on the transducer probe from outside the body.

There are multiple sources of error that affect strain imaging. Only axial displacement is considered in our elasticity imaging despite the presence of other displacement components. However, axial displacement is probably sufficient for distinguishing the tumorous region from the normal region since it is an elastic abnormality that we are detecting, not the absolute elasticity value. Decorrelation caused by deformation is another source of error in speckle tracking that causes error in creating displacement images. Hence decorrelation determines the upper preferred strain limit [13]. In this study, we used a pressure induced water injection by a syringe and a maximum displacement at the top of the phantom was less than 2 mm. This pressure and the displacement and strain it causes are well within the upper preferred strain limit.

5. CONCLUSIONS

Our prostate imaging approach combines using an I-Beam transducer with 3D capability, elasticity imaging and test on a prototype using a prostate tissue-mimicking phantom. The prostate strain imaging performed here using a slightly inflated sheath over the transrectal transducer significantly enhanced tumor visibility (a hard inclusion in the phantom). (The lesion was nearly invisible in the regular B-mode image.) The I-Beam transducer enabled reconstruction of discrete 2D image acquisitions into regular 3D grid space, and thus the tumor was rendered in 3D. The volume calculated for this tumor had an error of approximately 11% compared to the actual (independently determined) volume.

ACKNOWLEDGEMENTS

Siemens Medical Solutions provided the loan of a Sequoia 512 scanner with research (raw beamformer data) interface and provided technical support. Vermon SA (Tours, France) fabricated the transrectal I-Beam transducer. This work was partially financially supported by UVA Mellon Prostate Cancer Institute and the Department of Defense Prostate Cancer Research Program (PCRP) of the Office of Congressionally Directed Medical Research Programs (CDMRP) Grant number PC030402.

REFERENCES

1. Society, A.C., *Prostate Cancer Statistics from www.cancer.org*. 2004.
2. S. Alam, E.F., A. Kalisz, S. Ramchandran, R. Ennis, F. Lizzi, C.-S. Wu, and J. Ketterling, *In vivo Prostate Elastography: Preliminary Results*. Proceedings of IEEE Ultrasonics Symposium, 2004.
3. Pesavento, A. and A. Lorenz. *Real time strain imaging and in vivo applications in prostate cancer*. in *IEEE Ultrasonics Symposium*. 2001.
4. Ophir, J., et al., *Elastography: ultrasonic estimation and imaging of the elastic properties of tissues*. Proc. Institution of Mechanical Engineers, 1999. **213**(H): p. 203-233.
5. Erkamp, R., et al. *Exploiting strain-hardening of tissue to increase contrast in elasticity imaging*. in *IEEE Ultrasonics Symposium*. 2000.
6. Pesavento A, L.A., Ermert H, Sommerfeld H, Garcia-Schurmann M, Senge Th, Philippou S. *Frame-to-frame statistics of real-time strain images*. in *IEEE Ultrasonics Symposium*. 2000.
7. Hossack, J.A., et al., *Quantitative 3D Diagnostic Ultrasound Imaging Using a Modified Transducer Array and an Automated Image Tracking Technique*. IEEE Transactions on Ultrasonics Ferroelectrics & Frequency Control, 2002. **49**(8): p. 1029-1038.
8. Negron, L., et al., *Development and characterization of a vitreous mimicking material for radiation force imaging*. IEEE Transactions Ultrasonics, Ferroelectrics and Frequency Control, 2002. **49**(11): p. 1543-1551.
9. Hossack, J., T. Sumanaweera, and S. Napel. *Quantitative 3D Ultrasound Imaging Using an Automated Image Tracking Technique*. in *IEEE Ultrasonics Symposium*. 2000: IEEE.
10. Napel, S., et al., *Carotid Disease: Automated Analysis with Cardiac-gated Three-dimensional US Technique and Preliminary Results*. Radiology, 2002. **222**(2): p. 560-563.
11. Sarvazyan, A., *Mechanical imaging: a new technology for medical diagnostics*. Journal of Medical Informatics, 1998. **49**(2): p. 195-216.
12. R. W. Prager, R.N.R., et al, *Rapid Calibration For 3-D Freehand Ultrasound*. Ultrasound in Med. & Biol., 1998. **24**(6): p. 855-869.
13. Lubinski, M.A.E., S.Y.; O'Donnell, M., *Speckle tracking methods for ultrasonic elasticity imaging using short-time correlation*. Ultrasonics, Ferroelectrics and Frequency Control, IEEE Transactions on, 1999. **46**(1): p. 82 - 96.